

Fluorescence emission and anisotropy from rhodamine dimers

Thomas P. Burghardt^{*}, James E. Lyke, Katalin Ajtai

Department of Biochemistry and Molecular Biology, Mayo Foundation, Rochester, MN 55905, USA

Received 18 April 1995; revised 5 September 1995; accepted 6 September 1995

Abstract

The absorption, fluorescence emission, and excitation fluorescence anisotropy spectra of a rhodamine dye in a water–glycerol solution at high concentration were investigated to determine spectroscopic properties of the ground state dimer. The combination of data from these spectra measured at several dye concentrations contained sufficient constraints on the model for dimer association to permit an estimate of: the association constant, the extinction coefficients, the relative fluorescence quantum yield, and the emission spectra of the monomeric and dimeric species. The rhodamine dimer is an efficient fluorescence emitter with fluorescence anisotropy equivalent to that of the pure monomeric species over the range of excitation wavelengths covering its two lowest energy transitions.

Keywords: Rhodamine dimers; Fluorescence; Anisotropy; Lifetime; Quantum efficiency; Emission

1. Introduction

Rhodamine dyes are used as fluorescent probes of proteins in biological applications for detecting protein orientation because of their high time-zero anisotropy, photostability, and red emission making them ideal for use in a microscope. In muscle research, Borejdo et al. [1] observed time-resolved myosin cross-bridge rotation in active muscle fibers using fluctuations in polarized fluorescence from iodoacetamidotetramethylrhodamine (IATR) modifying the fast reacting thiol, SH1 (Cys 707), of myosin. Later, the steady-state linear dichroism of fluorescence from IATR on SH1 in fibers indicated that

cross-bridges in isometric contraction maintain a different orientation than those in rigor [2,3]. These observations conform with the notion that cross-bridges rotate to generate force during contraction. The special sensitivity of IATR to cross-bridge rotation is due principally to its unique orientation on the cross-bridge [4,5]. We observed the stereospecificity of IATR for the SH1 binding site on myosin by noting the differences in the efficiency between 5'-IATR and 6'-IATR for modification of SH1 [6]. At that time we also observed that the stoichiometry of the binding of 5'-IATR to SH1 was two probes per SH1 modification.

The affinity of rhodamine monomers for self-association is well known so it is reasonable to suspect that an IATR dimer could modify myosin. Characteristic for IATR-labeled myosin is a high (nearly maximal) fluorescence anisotropy covering the main

^{*} Corresponding author. Tel.: (507) 284 8120. Fax: (507) 284 9349. E-mail: burghardt@mayo.edu.

visible absorption band, when the labeled protein is randomly oriented and immobilized in a viscous solution. The high-anisotropy wavelength region includes the two visible transitions expected from a dimer such that, if a dimer is present, the transition dipoles are nearly parallel. Plane parallel or antiparallel, and stacked rhodamine monomers with single weakly coupled dipole oscillators is not a good model for the rhodamine monomer conformation in the dimer [7]. However, less symmetrical conformations with multiple weakly coupled oscillators (T.P. Burghardt and K. Ajtai, 1995, unpublished results), or vibronically (strongly) coupled oscillators could account for these observations [7]. In either case the fluorescence anisotropy of the coupled dipole oscillators in a dimer depends on the separation and relative orientation of the monomers by the dipole–dipole interaction. We investigated the fluorescence anisotropy of a model rhodamine dimer system by measuring the fluorescence emission and anisotropy of a rhodamine dye in solution where monomers and dimers are in equilibrium. We report here on methods for separating absorption and emission signals of monomeric from dimeric dye and on findings concerning the absorption, fluorescence emission, and fluorescence anisotropy of rhodamine dimers.

The formation of rhodamine dimers in solution begins at moderate concentrations of dye but the fraction of dimers to monomers is not near unity until ca. 3 mM dye concentration [8,9]. The observation of the emission from a dimer in solution is difficult because of the high concentrations needed and because the dimer is in equilibrium with the monomer. The emission from a highly absorbing solution of dye molecules is detected free of inner-filtering and self-absorption artifacts by using a very short path length capillary to contain the sample. The separation of monomer and dimer emission is managed by making a series of measurements in which we vary dye concentration and the excitation and emission wavelengths. A system of equations coupling the unknown monomer and dimer emission intensities or anisotropies describes the observed spectra. The unknowns are found with a least-squares protocol with inequality constraints.

We find that the rhodamine dimer emission is broader and red shifted relative to monomer emission, and that the quantum yield of the dimer is

slightly larger than that of the monomer. The fluorescence excitation anisotropy of the dimer is very nearly the same for the two lowest energy transitions in the dimer, as observed in rhodamine-labeled myosin, indicating that the planar, stacked rhodamine monomer conformation with two weakly coupled oscillators is not an appropriate model for the dimer. The observed dimer fluorescence anisotropy also appears inconsistent with origination from a vibronically induced, electronically forbidden, transition because the dimer's radiative lifetime is too similar to that of the monomer's electronically allowed transition. An alternative mechanism is proposed.

2. Materials and methods

2.1. Chemicals

Rhodamine 590 (R590) was from Exciton Inc. (Dayton, OH), spectrophotometric grade glycerol was from Aldrich (Milwaukee, WI), and spectroscopic grade ethanol (anhydrous alcohol) was from J.T. Baker (Phillipsburg, NJ).

2.2. Solutions

R590 was dissolved in a 40% glycerol–water mixture (volume-to-volume) at 0.4 mM, 0.2 mM, 0.1 mM, 0.01 mM, and 0.5 μ M probe concentrations. The glycerol volume was measured by weight using the glycerol density of 1.261 g/ml. R590 was dissolved in ethanol at 0.4 mM, 0.2 mM, 0.15 mM, 0.1 mM, 0.05 mM, and 0.5 μ M concentrations. In one experiment R590 was dissolved in 90% glycerol–water mixture at 1.0 μ M concentration.

2.3. Absorption spectroscopy

Absorption spectra were measured on a Cary 4 (Varian, Houston, TX) spectrophotometer using 0.02, 0.1, 0.2, or 1.0 cm path length cuvettes. Linearity of the Cary 4 is good to an optical density of ca. 3 without any special adaptation of the instrument. This was sufficient in all of our experiments. Absorption experiments on R590 in 40% glycerol–water solution were performed at 0°C. Experiments on R590 in ethanol were performed at 22°C.

We calculate absorption dipole strengths, $D_{0,m}$, for a transition from the ground state to excited state m , from the extinction coefficients using the formula [10]

$$D_{0,m} = 9.18 \times 10^{-3} \int \frac{\epsilon d\lambda}{(\beta^2/n)\lambda} (D^2) \quad (1)$$

where $\beta = (n^2 + 2)/3$, n is the refractive index of the medium containing the probe, and the limits of integration are set by the width of the absorption band of interest.

2.4. Fluorescence spectroscopy

We measured fluorescence spectra on an SLM 8000 fluorescence machine (SLM Instruments, Rochester, NY) equipped with Glan–Thompson polarizers. Emission intensity spectra were collected from 510 to 620 nm with a single grating monochromator without correction for the monochromator transmission or phototube response variability and with excitation wavelengths of 460, 480, 490, 500, and 510 nm. The slit widths were 2–4 nm on the excitation side and 4–8 nm on the emission side. Polarized emission, as a function of excitation wavelength, was detected at 519 ± 10 nm, 551 ± 5 nm, and 601 ± 5 nm emission wavelengths using a combination of cut-off and interference filters. Again the slit widths were 2–4 nm on the excitation side. We corrected all fluorescence spectra for lamp intensity and excitation monochromator transmission variations by dividing emission signals by the lamp intensity. The lamp intensity was detected with a 3 g/l solution of rhodamine B in ethylene glycol acting as a quantum counter. All fluorescence experiments on R590 in 40% glycerol–water solution were performed at 0°C. The fluorescence anisotropy experiment on 1.0 μ M R590 in 90% glycerol was performed at -15°C .

We measured high dye concentration fluorescence emission, without artifacts contributed by inner-filtering and/or self-absorption by using the capillary set-up shown in Fig. 1. The concentrated sample was drawn up in the rectangular glass capillary with dimensions $0.02 \times 0.002 \times 4$ cm (Vitro Dynamics, Rockaway, NJ). The capillary was mounted vertically in a 1-cm fluorescence cuvette and bathed in

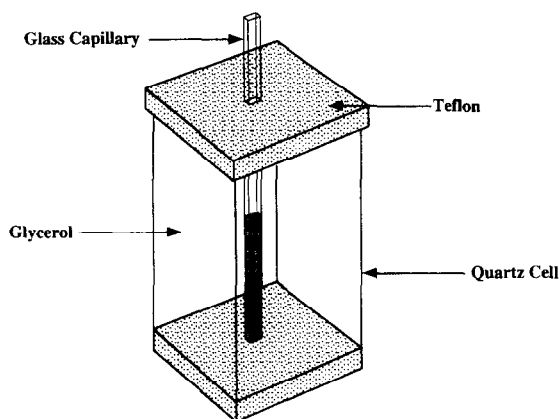


Fig. 1. The sample holder for a high concentration sample. A 0.02×0.002 cm rectangular glass capillary containing the sample is held at the center of a 1-cm quartz fluorescence cuvette containing 100% glycerol to minimize scattering of excitation light at the outer surface of the capillary. The capillary is oriented so that the excitation light beam propagates parallel to the longer path length.

100% glycerol to minimize scattering of excitation light at the outer surface of the capillary. We oriented the capillary so that the excitation light beam propagated parallel to the longer path length.

The capillary was narrow enough that all light emitted along the absorption path length, l , had equal probability of reaching the detection optics; however, the high concentration of the sample required that we used the full expression for absorbed light, A , such that

$$A = 1 - e^{-2.303\epsilon Cl} \quad (2)$$

where ϵ is the extinction coefficient, and C the absorber concentration. The emitted light was collected at right angles to excitation through the smallest dimension of the capillary.

We verified that artifacts from inner-filtering and/or self-absorption were negligible in the capillary set-up by comparing dimer forming samples to samples of R590 dissolved in ethanol. R590 in ethanol does not form aggregates as determined from the linearity of the absorption spectrum measured from R590 at 0.05–0.4 mM concentration as reported previously [8]. Thus, for R590 in ethanol, fluorescence emission spectral changes related to concentration that do not scale according to Eq. 2 are from inner-filtering and/or self-absorption artifacts but not from aggregation.

We calculated the overlap of absorption and emission spectra from monomeric R590, J_M , and dimer forming R590, J_D , to be able to compare observations of inner-filtering and self-absorption between monomeric R590 and dimer forming R590 such that

$$J_{M(D)} = \int A_{M(D)}(\lambda) f_{M(D)}(\lambda) d\lambda \quad (3)$$

where A is the absorption and f is the fluorescence quantum spectrum normalized to unity on the wavelength scale. f_M was measured from 0.5 μ M R590 in ethanol in a 1-cm cuvette where sample concentration artifacts were negligible. f_D was similarly measured from 0.5 μ M R590 in 40% glycerol where sample concentration artifacts and dimer formation were negligible. Comparing values of J for concentrations ≤ 0.4 mM gives $J_M > J_D$. Consequently, for concentrations ≤ 0.4 mM, when monomeric R590 is not inner-filtering or self-absorbing, then the dimer forming R590 is not inner-filtering or self-absorbing.

The emission observed from monomeric 0.4 mM R590 in the capillary scales with absorber concentration according to Eq. 2 and has a normalized emission spectrum identical to that from 0.5 μ M R590 in ethanol. In the latter sample there are no associated inner-filtering or self-absorption artifacts indicating the same for the high concentration monomeric sample and we conclude that our capillary system is free of these artifacts for the dimer forming samples when concentration is ≤ 0.4 mM.

The fluorescence anisotropy, r , is defined by

$$r \equiv \frac{F_{\parallel} - F_{\perp}}{F_{\parallel} + 2F_{\perp}} \quad (4)$$

where $F_{\parallel(\perp)}$ is the fluorescence emission intensity for light polarized \parallel (\perp) to the excitation light polarization. Polarized fluorescence intensities were corrected for differences in the efficiencies of light detection as a function of polarization by determining the factor g such that $g = F_{\parallel}/F_{\perp}$ when F is measured from a sample with zero anisotropy. Then F_{\perp} observed from samples with unknown anisotropy is corrected by multiplication with g before forming the anisotropy. We chose 0.5 μ M R590 in ethanol at 22°C as a suitable zero anisotropy sample.

3. Results and discussion

3.1. Choice of conditions

We looked for optimum conditions to study the fluorescence anisotropy of the R590 dimer. Ideally this called for high concentration of probe in a solvent that immobilized the molecules. We tried a glycerol–water mixture and found that glycerol significantly interfered with dimer formation when the mixture was greater than 40% glycerol. When we changed the temperature we found that temperatures lower than 0°C also interfered with dimer formation. The 40% glycerol–water mixture at 0°C is an optimum condition balancing dimer formation affinity and probe immobilization. The molecules are slowly tumbling under this condition so that the fluorescence anisotropy of the immobilized dimer is not directly measured from this sample. We compensated for dye mobility by applying a standard model for probe tumbling to convert the observed spectra to the anisotropy of the immobilized dimer [11].

3.2. Absorption measurements

Fig. 2 shows the effective extinction coefficients of R590 in 40% glycerol at four concentrations. We

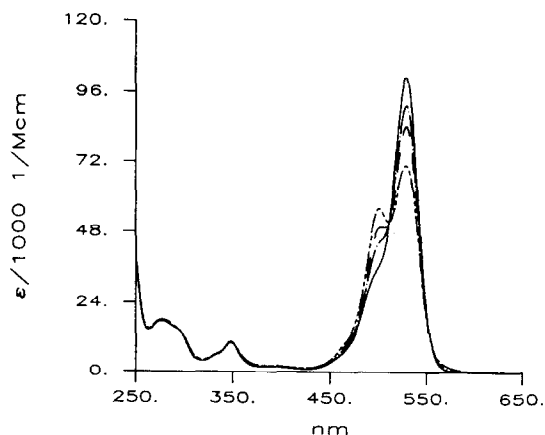


Fig. 2. The effective extinction coefficient of R590 in 40% glycerol formed by dividing the optical density by the product of the path length and dye concentration, $[M_0]$. The curves show increasing dimer formation for (—) $[M_0] = 0.01$ mM, (---) 0.1 mM, (- - -) 0.2 mM, and (· · ·) 0.4 mM.

modeled the interaction of the dye molecules as a bimolecular reaction such that



where M is a monomer, D is a dimer, k_i is a reaction rate, and $C = k_1/k_2$ is the association constant. At equilibrium, the absorption of a dye solution with concentration $[M_0]$ is

$$A = \varepsilon_M[M]l + \varepsilon_D[D]l \quad (6)$$

where $\varepsilon_{M(D)}$ is the monomer (dimer) extinction coefficient and l the path length. The concentrations at equilibrium are

$$[M] = \sqrt{[D]/C}$$

and

$$[D] = 1/8 \left\{ x - \sqrt{x^2 - 16[M_0]^2} \right\}$$

where $x = 4[M_0] + 1/C$ [12]. The unknowns in Eq. 6 are the linear coefficients ε_M , ε_D , and the non-linear quantity C (implicit in Eq. 6). We used Eq. 6 and a least-squares protocol on the spectra in Fig. 2 to find the best estimates of ε_M and ε_D , for a given C . The least-squares protocol included inequality constraints such that ε_M and ε_D were ≥ 0 . We found the best choice for C by minimizing the sum of the χ^2 values from every wavelength in the spectrum while searching through a reasonable domain for C . The solution specifies C and the extinction coefficients as a function of wavelength. In 40% glycerol at 0°C, we found that $C = 1010 \pm 100 \text{ M}^{-1}$ which is ca. half its value for R590 in water at room temperature. From C we calculated that at $[M_0] = 0.1 \text{ mM}$, $[M] = 8.53 \times 10^{-5} \text{ M}$, and $[D] = 7.35 \times 10^{-6} \text{ M}$, and that at $[M_0] = 0.4 \text{ mM}$, $[M] = 2.62 \times 10^{-4} \text{ M}$, and $[D] = 6.92 \times 10^{-5} \text{ M}$. These values are used in the interpretation of the fluorescence experiments described in Section 3.3.

Fig. 3 shows the best estimates of ε_M and ε_D for R590. In the figure $0.5\varepsilon_D$ is drawn so that the two curves have similar peak values. The longest wavelength absorption band of the monomer with dipole strength 64.7 D^2 splits into two bands with dipole strengths 13.5 and 102.8 D^2 in the dimer. The sum of the two dimer dipole strengths is less than twice the monomer dipole strength indicating that these

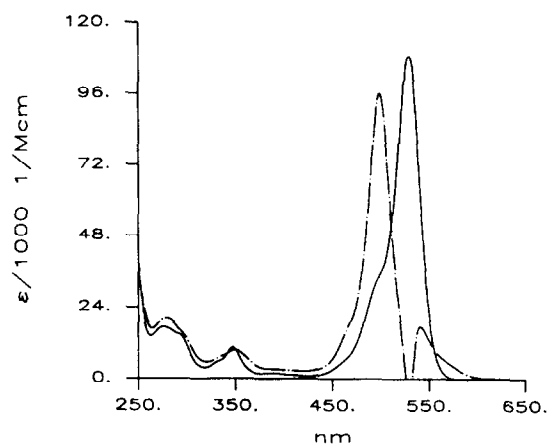


Fig. 3. The extinction coefficient of the R590 monomer, ε_M (—), and the dimer, $1/2\varepsilon_D$ (---), calculated from the curves shown in Fig. 1. The curves indicate equal dipole strengths (computed using Eq. 1) for the excitation wavelength domain shown.

dimer bands are hypochromic so that other electronic transitions in the monomers are participating in the coupled dipole interaction. The dimer extinction coefficient indicates that light near to 530 nm is absorbed exclusively by the monomer.

3.3. Fluorescence emission intensity measurements

Shown in Fig. 4 are emission spectra from 0.1 mM and 0.4 mM R590 in 40% glycerol at an

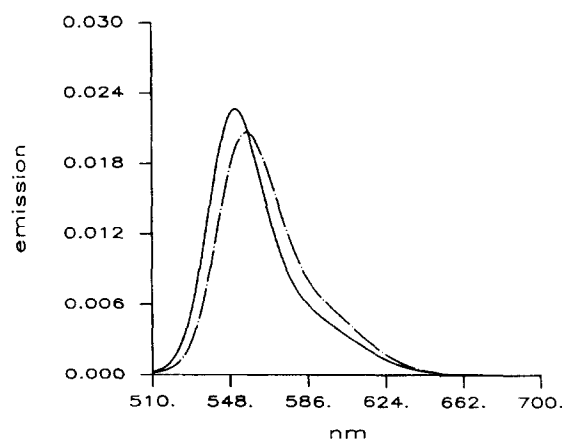


Fig. 4. The normalized Gaussian fit to fluorescence emission from (—) 0.1 mM and (---) 0.4 mM R590 in 40% glycerol at 0°C and excited with 500 nm light. Measurements were carried out with the capillary set-up shown in Fig. 1. The curves shown are 3–4 Gaussian functions best fitted to the observed data.

excitation wavelength of 500 nm where both monomeric and dimeric species are absorbing light. Both spectra were measured using the capillary set-up shown in Fig. 1. The emission from the higher concentration of dimers present in the 0.4 mM compared to the 0.1 mM R590 sample causes the observed spectral shift.

We modeled the fluorescence intensity, F , of the dye molecules in terms of normalized fluorescence quantum spectra for monomer and dimer emission, $f_M(\lambda)$ and $f_D(\lambda)$, and included the possibility of excitation transfer by the Förster mechanism and by the collision of molecules. It is shown in Appendix A that the normalized fluorescence intensity from the dye solution is given by Eq. A24 such that

$$F/F_0 = A_D Q_{D,T} f_D(\lambda) + A_M Q_{M,T} f_M(\lambda) \quad (7)$$

where from Eq. 2, $A_D = 1 - \exp(-2.303 \epsilon_D [D] l)$ and $A_M = 1 - \exp(-2.303 \epsilon_M [M] l)$, and where $Q_{(D,M),T}$ is the quantum efficiency for emission by the dimer (monomer) given explicitly in Eqs. A19–23 and A25.

F is divided by $Q_{D,T}$ and normalized such that

$$\mathcal{F} = \frac{F}{\int F d\lambda} = \frac{af_M + bf_D}{a + b} \quad (8)$$

where

$$a = A_M Q_{M,T} / Q_{D,T} \quad b = A_D \quad (9)$$

$$\int f_M d\lambda = 1 \quad \int f_D d\lambda = 1 \quad (10)$$

and integration is over all emission wavelengths.

The unknowns in Eqs. 8–10 are the linear coefficients f_M , f_D , and the ratio $Q_{M,T}/Q_{D,T}$. $Q_{M,T}/Q_{D,T}$ depends on the unknown non-linear factors: $Q_{M,0}/Q_{D,0}$, the ratio of quantum efficiencies in the absence of any form of energy transfer (see Eq. A23), δ_D and δ_M , the factors affecting the back transfer rate of energy following self-energy transfer (see Eqs. A8–9), and the collisional quenching constants (see Eq. A22). We measured emission spectra like those shown in Fig. 4 for $[M_0] = 0.1$ mM or 0.4 mM and with excitation wavelengths of 460, 480, 490, 500, and 510 nm for a total of 10 emission spectra. The excitation wavelengths selected cover the visible absorption bands of both monomer and dimer. We used Eq. 8 and a least-squares protocol on these emission spectra to find the best estimate of f_M and f_D , for given $Q_{M,T}/Q_{D,T}$, but assuming all

Förster energy transfer is absent. Using this lowest order estimate of f_D and f_M , the characteristic energy transfer distances are computed and new best estimates for f_D and f_M , that include Förster energy transfer, are generated. This iterative process is repeated until it is self-consistent.

The least-squares protocol included inequality constraints requiring f_M and $f_D \geq 0$. We found the best choices for the non-linear unknowns by searching through reasonable domains for their values while minimizing the sum of the χ^2 values from every wavelength in the spectrum. The χ^2 values were unaffected by any reasonable choices for the collisional quenching constants so that these parameters are unknown but may be set to zero. The χ^2 values are very mildly affected by the choice of δ_D and δ_M and suggest that $\delta_D \approx 1$ and $\delta_M \approx 0$. These values for δ_D and δ_M indicate that for the monomer Förster self-energy transfer is irreversible while for the dimer it is fully reversible. The χ^2 values are sensitive to the choice of $Q_{M,0}/Q_{D,0}$ and suggest that $Q_{M,0}/Q_{D,0} = 0.9 \pm 0.1$, indicating that in solution the dimer is a slightly more efficient fluorescence emitter than the monomer. We also found that the Förster characteristic distances for donor \rightarrow acceptor transfer are $R_0(M \rightarrow M) = 44.0$ Å, $R_0(M \rightarrow D) = 41.6$ Å, $R_0(D \rightarrow D) = 38.7$ Å, and $R_0(D \rightarrow M) = 33.3$ Å.

Comparison of the f_D and f_M computed before and after inclusion of Förster energy transfer indicates that it contributes negligibly to the emission shapes and quantum efficiencies. Our treatment of this effect, described in Appendix A, is correct to only zeroth order from neglecting the off-diagonal elements of the matrix governing excited state relaxation, see Eq. A11. Physically this is equivalent to treating the Förster energy transfer crossing from monomer to dimer or from dimer to monomer as a radiationless quenching process. We applied perturbation theory to estimate the importance of the off-diagonal elements of the relaxation matrix and found that the next order of approximation produced no observable change in f_D and f_M .

Fig. 5 shows the best estimates of f_M and f_D for the R590. Dimer emission is broader and red shifted when compared to the monomer emission. These curves indicate that the blue edge of the spectrum is exclusively the monomer emission and that there is

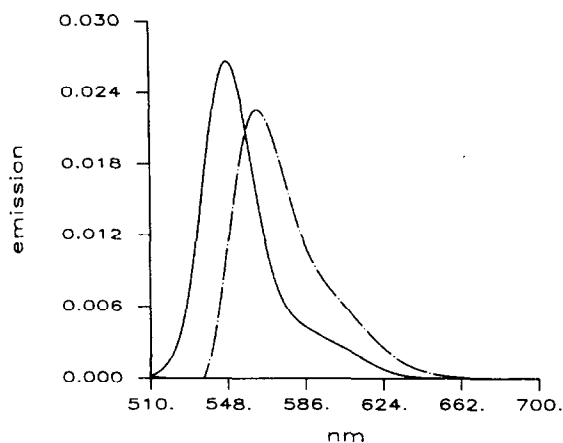


Fig. 5. The normalized fluorescence quantum spectrum from the R590 monomer, f_M (—), and dimer, f_D (---).

no region where dimer emission is exclusive. The Stokes shift, $\Delta S \approx 19$ nm in the monomer and 22 nm in the dimer. The dimer shift is measured from the lowest energy absorption peak at 541 nm to the dimer emission peak at 563.0 nm. The difference in ΔS indicates a change in the difference between the excited and ground state dipoles for the monomer compared to the dimer.

3.4. Fluorescence anisotropy of the dimer

Fig. 6 shows the excitation fluorescence anisotropy from R590 in 90% glycerol and in 40% glycerol. The anisotropy in the 90% glycerol solution is from a monomeric immobilized probe while in the 40% glycerol solution the anisotropy is from a mixture of slowly tumbling monomers and dimers. We modeled the fluorescence anisotropy, r , from the mixture of monomeric and dimeric dye molecules in terms of monomer and dimer anisotropies, r_M and r_D , respectively. Using the anisotropy sum rule relating the contributions to r from the component anisotropies we find that

$$r = \frac{A_M Q_M f_M r_M + A_D Q_D f_D r_D}{A_M Q_{M,T} f_M + A_D Q_{D,T} f_D} \quad (11)$$

where Q_M and Q_D are defined in Eq. A22 and represent the quantum efficiencies for monomer and dimer emission in the absence of Förster energy transfer, and the coefficients multiplying the component anisotropies are the fractional emission intensi-

ties. The anisotropies involving emission following energy transfer, for instance $r_{D \rightarrow M}$ and $r_{M \rightarrow D}$, are assumed to be zero due to the depolarization upon energy transfer. Eq. 11 is appropriate for immobilized samples but since our dye molecules in 40% glycerol are mobile on the time scale of probe lifetime we alter it to account for this mobility by renormalizing the fractional intensity coefficients such that [11]

$$r = g_M r_M + g_D r_D \quad (12)$$

where

$$g_M = \frac{A_M Q_M f_M}{(A_M Q_{M,T} f_M + A_D Q_{D,T} f_D)(1 + \Omega_{M,T})}$$

$$g_D = \frac{A_D Q_D f_D}{(A_M Q_{M,T} f_M + A_D Q_{D,T} f_D)(1 + \Omega_{D,T})} \quad (13)$$

$$\Omega_{M,T} = \Omega_{M,0} Q_{M,T} / Q_{M,0} \quad \Omega_{D,T} = \Omega_{D,0} Q_{D,T} / Q_{D,0} \quad (14)$$

$$\Omega_{M,0} = \tau_{F,M} Q_{M,0} / \phi_M \quad \Omega_{D,0} = \tau_{F,D} Q_{D,0} / \phi_D \quad (15)$$

$Q_{i,0}$ is the concentration independent quantum efficiency defined in Eqs. A22–23, $\tau_{F,i}$ is the radiative lifetime, and ϕ_i is the rotational correlation time of the molecule. In Eqs. 14 and 15 only $Q_{i,T}$ is concen-

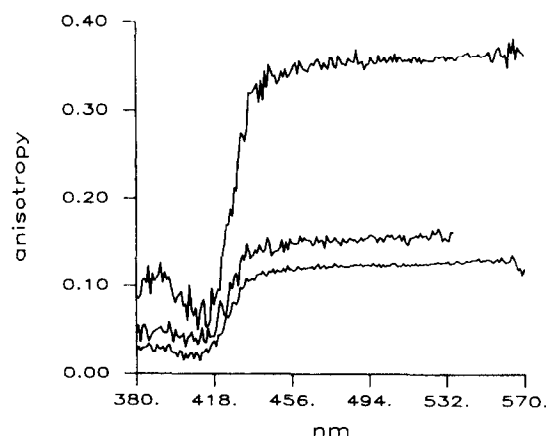


Fig. 6. The excitation fluorescence anisotropy spectrum from monomeric R590 in 90% glycerol with emission wavelength 605 nm (top), from a monomeric R590 in 40% glycerol with an emission wavelength of 551 nm (middle), and from a mixture of monomeric and dimeric R590 in 40% glycerol with an emission of 601 nm (bottom). The monomeric 90% glycerol sample is fully immobilized. The 40% glycerol samples are slowly tumbling.

tration dependent. The unknowns in Eq. 12 are the linear coefficients r_M , r_D , and the normalizations $1 + \Omega_{M,T}$ and $1 + \Omega_{D,T}$. Given $\Omega_{M,0}$ and $\Omega_{D,0}$, then $\Omega_{M,T}$ and $\Omega_{D,T}$ are computed using the information obtained from the emission spectra discussed in Section 3.3.

We measured excitation fluorescence anisotropy spectra like those shown in Fig. 6 for $[M_0] = 0.5 \mu\text{M}$ or 0.4 mM and for the three emission wavelengths $519 \pm 10 \text{ nm}$, $551 \pm 5 \text{ nm}$, and $601 \pm 5 \text{ nm}$ for a total of six spectra of R590 in 40% glycerol. The low concentration sample was measured in a standard 1-cm square cuvette. The 0.4 mM sample was measured using the capillary set-up shown in Fig. 1. The emission wavelengths selected cover the emission bands of both the monomer and dimer. We used Eq. 12 and a least-squares protocol on these polarization spectra to find the best estimate of r_M and r_D , for given $\Omega_{M,0}$ and $\Omega_{D,0}$. The least-squares protocol included inequality constraints such that $-0.2 \leq r_M, r_D \leq 0.4$. Because the Ω 's are practically linear parameters in the anisotropy the sum of the χ^2 values from every wavelength in the excitation polarization spectrum was independent of the choice of $\Omega_{M,T}$ and $\Omega_{D,T}$ so that we needed additional information to determine these quantities.

The limiting anisotropy of the monomer species, $r_{M,\text{max}}$, was estimated from the excitation polariza-

tion spectrum in Fig. 6 for R590 in 90% glycerol to be 0.37. We assumed that the limiting anisotropy of the dimer $r_{D,\text{max}} = r_{M,\text{max}}$ and adjusted $\Omega_{M,0}$ and $\Omega_{D,0}$ to give these values for the limiting anisotropies in the least-squares solution to Eq. 12 and found $\Omega_{M,0} \approx 1.4$ and $\Omega_{D,0} \approx 2.1$. Fig. 7 shows the resolved monomer and dimer fluorescence anisotropies for immobilized molecules. Both spectra show anomalous behavior around excitation at 530 nm. These anomalies are artifacts due to the vanishing of our estimate for ε_D in the vicinity of this wavelength.

3.5. Implications for dimer structure and spectroscopy

The dimer anisotropy maintains a large value close to its limiting value of 0.37 over an excitation range that includes both the long-wavelength absorption bands of the dimer as observed previously for a rhodamine dimer under very different conditions [7]. It was also pointed out previously that the simplest exciton coupling model using two electronic states coupled with a dipole–dipole interaction for a dimer conformation of planar, stacked xanthene rings was unable to account for the absorption and fluorescence data in rhodamine [7]. One demonstrated alternative is to involve vibronic coupling in the dimer interaction [7,13,14]. Another is to generalize the exciton coupling model to include higher energy electronic transitions in the rhodamine monomer and to allow the planar structure to stack asymmetrically in a staircase-like structure. With the latter model it is possible to show that the anisotropy of the two lowest energy transition moments need not be perpendicular. We are also able to semi-quantitatively account for the absorption and emission anisotropy data provided the model includes two dimer conformations in equilibrium (T.P. Burghardt and K. Ajtai, 1995, unpublished results). We will motivate and discuss this possibility further below. However, independent of the model chosen, the observed hypochromism in the lowest energy transitions of the dimer indicates that higher energy monomer electronic states are coupled to the lowest energy states by the dipole–dipole interactions in the dimer.

We investigate further the significance of our findings regarding the intramolecular interactions in

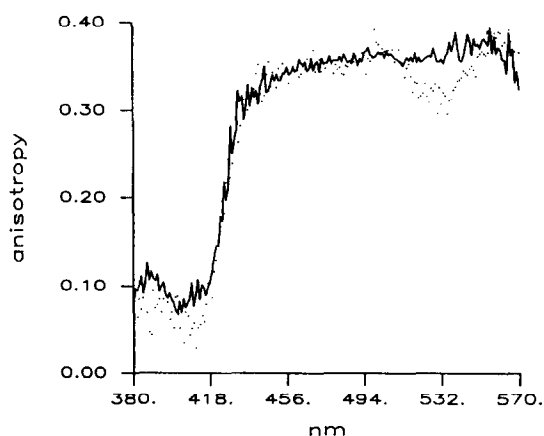


Fig. 7. The excitation fluorescence anisotropy spectrum of R590 monomers, r_M (—), and dimers, r_D (···). The dip near $\lambda_{\text{ex}} = 530 \text{ nm}$ originates from an anomaly explained in the text.

the dimer using Eqs. 14 and 15 and the ratio of the radiative lifetimes, T , such that

$$T \equiv \frac{\tau_{F,D}}{\tau_{F,M}} = \frac{\Omega_{D,0}}{\Omega_{M,0}} \frac{Q_{M,0}}{Q_{D,0}} \frac{\phi_D}{\phi_M} \quad (16)$$

We can evaluate the right hand side (rhs) of Eq. 16, using the fluorescence intensity and anisotropy data presented in Sections 3.3 and 3.4, provided we can estimate the ratio of relaxation times, $R = \phi_M/\phi_D$. We modeled the monomeric and dimeric molecules as oblate ellipsoids of revolution and used the Perrin equations to estimate R . This calculation is described in Appendix B where we show that $R \approx 0.69$. Then the ratio of the radiative lifetimes, T_F , estimated from the emission data, R , and Eq. 16 gives $T_F \approx 1.9$. This is an upper limit on T_F since we have assumed that $r_{D,max} = r_{M,max}$ while $r_{M,max}$ is practically the maximum allowed theoretically. If $r_{D,max} \leq r_{M,max}$ then T_F will be smaller so that $T_F \leq 1.9$. Alternatively, T can be estimated directly from the absorption spectra of Fig. 3 such that, $\tau_{F,M}/\tau_{F,D} = \nu_D^3 \Delta_D / \nu_M^3 \Delta_M$, where ν_i and Δ_i stand for the peak frequency and dipole strength of the lowest energy transition of species i [11]. Then the ratio of radiative lifetimes, T_A , estimated from the absorption spectra gives $T_A \approx 4.7$, in rough agreement with previous observations [7].

These estimates for T differ by more than a factor of 2. The emission data favors a smaller estimate for the dimer radiative lifetime suggesting that $\tau_{D,F} \leq 2\tau_{M,F}$ and consistent with the notion that the lowest energy transition in the dimer is an electronically allowed transition. Alternatively, the absorption data favors a larger estimate for the dimer radiative lifetime suggesting that $\tau_{D,F} \approx 5\tau_{M,F}$ and consistent with the notion that the lowest energy transition in the dimer corresponds to a vibronically induced, electronically forbidden, transition [7]. A model accounting for these findings has the dimer data originating from two dimer conformations in solution. One dimer conformation, structure **B**, has an allowed transition at the lowest energy band in the dimer absorption spectrum. When it is excited it relaxes with a radiative lifetime ca. 1/2 the monomer radiative lifetime. Structure **B** is the minority constituent of the dimer population at equilibrium. The other dimer confor-

mation, structure **A**, with a forbidden lowest energy transition, has a long radiative lifetime so that the change from structure **A** to **B** is the principal mechanism for deexcitation. Structure **A** is the major constituent of the dimer population at equilibrium. The observed radiative lifetime from the mixture of **A** and **B** dimers, derived from emission data, would be in between the extremes of the allowed and forbidden electronic transitions and would depend on the rate at which structure **A** converts to **B**. The observed dimer radiative lifetime, derived from the absorption data, would indicate the radiative lifetime of structures **A** and **B** times their fractional concentration.

Consider the structure **A** to **B** conversion as a mechanism for deexcitation of an excited dimer in a forbidden transition state. We model this process approximately by altering the dimer radiative rate such that, $k_{F,D} \rightarrow (1 - p_{A \rightarrow B})k'_{F,D} + p_{A \rightarrow B}k''_{F,D}$, where $k'_{F,D}$ is the forbidden transition dimer radiative rate, $k''_{F,D}$ is the allowed transition dimer radiative rate, and $p_{A \rightarrow B}$ is the probability of conversion of the dimer conformations. Then from Eq. 16 and the emission data

$$\frac{\tau'_{F,D}}{1 - p_{A \rightarrow B} + p_{A \rightarrow B}\tau'_{F,D}/\tau''_{F,D}} \leq 2\tau_{F,M} \quad (17)$$

where $\tau'_{F,D} = 1/k'_{F,D}$ and $\tau''_{F,D} = 1/k''_{F,D}$. Solving for $p_{B \rightarrow A}$ we find

$$p_{A \rightarrow B} \geq \frac{(\tau'_{F,D}/2\tau_{F,M}) - 1}{(\tau'_{F,D}/\tau''_{F,D}) - 1} \quad (18)$$

If $\tau'_{F,D} \approx 8\tau_{F,M}$, as suggested previously [7], and $\tau''_{F,D} \approx 1/2\tau_{F,M}$ for an allowed dimer transition then we obtain $p_{A \rightarrow B} \geq 0.2$, supporting the notion that the interconversion of the dimer structures is a significant mechanism for dimer emission.

Our analysis of dimer absorption and emission did not distinguish between the physical properties of the proposed two dimeric species, **A** and **B**. A more elaborate model for dimer formation would include the two distinguishable dimers and the possibility of interconversion between species. The above discussion, based on a single dimer species model, shows that two dimeric species must be introduced to rationalize differing estimates of the dimer radiative life-

time. The generalized model would necessarily agree with this observation and perhaps furnish an estimate, rather than an lower bound, for $p_{B \rightarrow A}$.

4. Conclusions

The spectroscopic properties of the rhodamine dimer in solution were investigated under conditions where the monomer and dimer conformers were in equilibrium. Using methods we developed to separate the spectroscopic contributions of monomers and dimers we found that the dimer is fluorescent with a quantum efficiency about equal to the monomer. Polarized emission from the dimer indicates that the two lowest energy transitions have dipoles nearly parallel to the emission dipole. The radiative lifetime of the dimer, indicated by the fluorescence emission data, is near to that of the monomer and much shorter than that indicated by the dimer dipole strength. It appears that the dimer conformation consists of two forms in equilibrium. One form, the minor component, possesses an allowed electronic transition at the lowest transition energy. The second form, the major component, possesses an electronically forbidden transition at this energy but interconversion between the dimer conformers allows the second form to fluoresce efficiently.

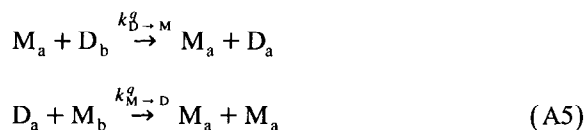
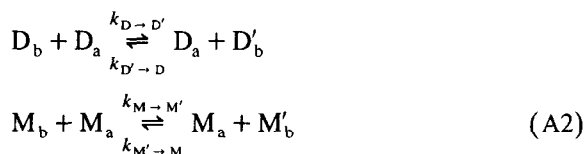
Acknowledgements

We thank Ms. Jacqueline Lafky for help with drawing the figures. This work was supported by National Institutes of Health Grant R01 AR 39288, the American Heart Association Grant-In-Aid 930 06610, and by the Mayo Foundation.

Appendix A. Energy transfer among monomers and dimers in solution

A solution of monomer and dimer fluorophores is in equilibrium. Relaxation from the excited state singlet is accomplished by fluorescence, collisional energy transfer, and Förster energy transfer. This

process is modeled by the kinetic equations deduced from the reaction steps



where subscript b(a) refers to the excited (ground) state, $k_{F,D(M)}$ is the dimer (monomer) radiative decay rate, and $k_{S,D(M)}$ is the dimer (monomer) decay rate for processes other than radiative. Both k_F and k_S are independent of fluorophore concentration. We assume that the difference between the primed and unprimed species is that the back transfer rate can be different from the forward rate. The light emission from either species is equivalent so we substitute $k_{D' \rightarrow D} = \delta_D k_{D \rightarrow D'}$ and $k_{M' \rightarrow M} = \delta_M k_{M \rightarrow M'}$ and the primes are dropped. The rate equations for D_b and M_b are then

$$dD_b/dt = -\gamma_D D_b + k_{M \rightarrow D} D_a M_b + k_D^{-1} D_a \quad (A6)$$

$$dM_b/dt = -\gamma_M M_b + k_{D \rightarrow M} M_a D_b + k_M^{-1} M_a \quad (A7)$$

where

$$\begin{aligned} \gamma_D &= k_{F,D} + k_{S,D} + (1 - \delta_D) k_{D \rightarrow D} D_a + k_{D \rightarrow M} M_a \\ &\quad + k_{D \rightarrow D}^g D_a + k_{D \rightarrow M}^g M_a \end{aligned} \quad (A8)$$

$$\begin{aligned} \gamma_M &= k_{F,M} + k_{S,M} + (1 - \delta_M) k_{M \rightarrow M} M_a \\ &\quad + k_{M \rightarrow D} D_a + k_{M \rightarrow M}^g M_a + k_{M \rightarrow D}^g D_a \end{aligned} \quad (A9)$$

Assuming D_a and M_a are constant, Eqs. A6–7 become first order and they are put in standard form with the substitutions $D_b = x_1 + \beta_1$ and $M_b = x_2 + \beta_2$ where

$$\beta_1 = D_a \frac{k_D^{-1} \gamma_M + k_M^{-1} M_a k_{M \rightarrow D}}{k_{D \rightarrow M} M_a k_{M \rightarrow D} D_a - \gamma_M \gamma_D}$$

$$\beta_2 = M_a \frac{k_M^{-1} \gamma_D + k_D^{-1} D_a k_{D \rightarrow M}}{k_{D \rightarrow M} M_a k_{M \rightarrow D} D_a - \gamma_M \gamma_D} \quad (A10)$$

Then $dv/dt = Av$ where $v = (x_1, x_2)$ and

$$A = \begin{pmatrix} -\gamma_D & k_{M \rightarrow D} D_a \\ k_{D \rightarrow M} M_a & -\gamma_M \end{pmatrix} \quad (A11)$$

Neglecting off-diagonal elements in A for the lowest order solution and for an initial condition caused by a delta function pulse of excitation light we find

$$D_b(t) = D_b(0) \exp(-\gamma_D t)$$

$$M_b(t) = M_b(0) \exp(-\gamma_M t) \quad (A12)$$

Energy transfer rates $k_{D \rightarrow D}$, $k_{D \rightarrow M}$, $k_{M \rightarrow M}$, and $k_{M \rightarrow D}$ represent both collisional and Förster energy transfer processes. Below we consider only Förster transfer but it is a simple generalization of these arguments to include the possibility of collisional transfer. We reexpress the relaxation rates, γ_D and γ_M from Eqs. A8–9, in terms of lifetimes and the distance between donor and acceptors in the Förster energy transfer rates giving

$$\gamma_D(t) = (1/\tau_D) \left\{ 1 + \sum_{i=1}^{N_M} [R_0(D \rightarrow M)/R_i]^6 + (1 - \delta_D) \sum_{i=1}^{N_D} [R_0(D \rightarrow D)/R_i]^6 \right\} \quad (A13)$$

$$\gamma_M(t) = (1/\tau_M) \left\{ 1 + \sum_{i=1}^{N_D} [R_0(M \rightarrow D)/R_i]^6 + (1 - \delta_M) \sum_{i=1}^{N_M} [R_0(M \rightarrow M)/R_i]^6 \right\} \quad (A14)$$

where

$$\tau_D = 1/(k_{F,D} + k_{S,D} + k_{D \rightarrow D}^q D_a + k_{D \rightarrow M}^q M_a) \quad (A15)$$

$$\tau_M = 1/(k_{F,M} + k_{S,M} + k_{M \rightarrow M}^q M_a + k_{M \rightarrow D}^q D_a) \quad (A16)$$

R_0 is the characteristic energy transfer distance for the indicated donor–acceptor pair, and R_i is the distance from the donor to the i th acceptor. R_0 depends implicitly on the concentrations of D_a and M_a through the donor quantum efficiency in the absence of acceptor [18].

We evaluate the quantum efficiency for dimer or monomer emission by considering the probability, $\rho(t)$, that a dimer or monomer donor excited at $t = 0$ remains excited at time t given by [16,17]

$$\rho_{D(M)}(t) = \exp[-(t/\tau_{D(M)})\gamma_{D(M)}] \quad (A17)$$

The total quantum efficiency for dimer (monomer) emission, $Q_{D(M),T}$, is then

$$Q_{D(M),T} = k_{F,D(M)} \int_0^\infty dt \rho_{D(M)} \quad (A18)$$

By ensemble averaging $Q_{D(M),T}$ over the acceptors with manipulations described by Förster [16] we obtain¹

$$Q_{D(M),T} = Q_{D(M)} \left[1 - \sqrt{\pi} q_{D(M)} \times \exp(q_{D(M)}^2) \Phi(q_{D(M)}) \right] \quad (A19)$$

where

$$q_D = 1/2\sqrt{\pi} \left\{ [M] R_0^3(D \rightarrow M) + \sqrt{1 - \delta_D} [D] R_0^3(D \rightarrow D) \right\} \quad (A20)$$

$$q_M = 1/2\sqrt{\pi} \left\{ [D] R_0^3(M \rightarrow D) + \sqrt{1 - \delta_M} [M] R_0^3(M \rightarrow M) \right\} \quad (A21)$$

$$Q_D = \frac{Q_{D,0}}{1 + k_{D \rightarrow D}^q \tau_{D,0} D_a + k_{D \rightarrow M}^q \tau_{D,0} M_a}$$

¹ The root mean square (rms) distance traveled by a diffusing particle in time τ , $r \approx \sqrt{6D\tau}$. The diffusion constant for rhodamine in water at 20°C, $D_{20,w} \approx 4 \times 10^{-6}$ cm²/s [11]. Conversion to our conditions is accomplished with $D = D_{20,w}(273/293)(1.002/8.250) = 4.5 \times 10^{-7}$ cm²/s where the first fraction is the ratio of absolute temperatures at 0 and 20°C and the second is the ratio of the viscosities of water at 20°C to that of 40% glycerol at 0°C [11,15]. Then rhodamine diffuses 7–10 Å during the 2–4 ns lifetime of the probe [6]. The average distance between molecules in the highest concentration sample of 0.4 mM is ca. 200 Å indicating that the dye molecules are statically distributed during the dye lifetime. Statically distributed acceptors is implicit in the method of acceptor averaging applied here to arrive at Eqs. A19–A23.

$$Q_M = \frac{Q_{M,0}}{1 + k_{M \rightarrow M}^q \tau_{M,0} M_a + k_{M \rightarrow D}^q \tau_{M,0} D_a} \quad (A22)$$

$$Q_{D(M),0} = \frac{k_{F,D(M)}}{k_{F,D(M)} + k_{S,D(M)}}$$

$$1/\tau_{D(M),0} = k_{F,D(M)} + k_{S,D(M)} \quad (A23)$$

[D] and [M] are the equilibrium concentrations of the dimers and monomer, and the error function

$$\Phi(q) \equiv (2/\sqrt{\pi}) \int_0^q dx \exp(-x^2)$$

Finally the observed normalized, steady-state fluorescence from a mixture of monomers and dimers, F/F_0 , in terms of normalized fluorescence quantum spectra for monomer and dimer emission, $f_M(\lambda)$ and $f_D(\lambda)$, is

$$F/F_0 = A_D Q_{D,T} f_D(\lambda) + A_M Q_{M,T} f_M(\lambda) \quad (A24)$$

where $A_{D(A)}$ is the light absorbed by the dimer (monomer) species.

Computation of F/F_0 for comparison with the observed signal is carried out using the characteristic transfer distance, R_0 , where

$$R_0 = 9.79 \times 10^3 (\kappa^2 n^{-2} QJ)^{1/6} (\text{\AA}) \quad (A25)$$

and κ^2 is the orientation factor, n the index of refraction of the medium containing the dye, Q the quantum efficiency of the donor in the absence of the acceptor, and J the overlap integral. In all calculations we assume $\kappa^2 = 2/3$ and $n = 1.380$ for the 40% glycerol–water solution at 0°C [15]. The radiative lifetime of the rhodamine monomer, $\tau_{F,M} = 8$ ns for a dipole strength of $64.7 D^2$ at 530 nm, and the fluorescence lifetime $\tau_{M,0} \approx 2$ ns [6], gives a quantum efficiency of the isolated rhodamine monomer in solution of $Q_{M,0} = 0.25$. The unknowns in Eqs. A19–25 are the emission spectral shapes f_D and f_M , the dimer quantum efficiency $Q_{D,0}$, the factors δ_D and δ_M affecting the back transfer rate of energy following self-energy transfer, and the collisional quenching constants $k_{D \rightarrow D}^q \tau_{D,0} D_a$, $k_{D \rightarrow M}^q \tau_{D,0} M_a$, $k_{M \rightarrow M}^q \tau_{M,0} M_a$, and $k_{M \rightarrow D}^q \tau_{M,0} D_a$.

Appendix B. Rotational relaxation times of an oblate ellipsoid

An oblate ellipsoid approximates the shape of the R590 molecule. The major axis, a , measured from

the center of the xanthene to the end of one of the diethyl side groups is ≈ 7 Å, and the minor axis, b , giving the dimension perpendicular to the plane of the xanthene ring, is ≈ 3 Å. It was suggested that the rhodamine dimer has stacked xanthene rings with a head-to-head conformation [9,19]. In this conformation the dimer has about the same major axis dimension as the monomer but double the minor axis dimension. The oblate ellipsoid has a volume $V = 4\pi a^2 b$, so that the dimer volume is double that of the monomer.

The Perrin equations give the two rotational relaxation rates of an oblate ellipsoid as a function of volume and the ratio of major to minor axis dimensions, p [11]. The rotational relaxation times for motion of major axis, ϕ_a , and the minor axis, ϕ_b , are

$$\phi_a = \frac{2\alpha V}{[1/f_a + 1/f_b]} \quad \phi_b = \alpha V f_a \quad (B1)$$

where f is the frictional coefficient given by

$$f_a = \frac{4(1-p^2)}{3(2-Sp^2)} \quad f_b = \frac{4(1-p^4)}{3p^2[S(2-p^2)-2]} \quad (B2)$$

$$S = 2(p^2 - 1)^{1/2} \tan^{-1}[(p^2 - 1)^{1/2}] \quad (B3)$$

$$p = a/b \quad (B4)$$

and α is a proportionality constant. The static fluorescence polarization detects the harmonic mean of the two relaxation times, ϕ_h , such that

$$\phi_h = \frac{3}{[2/\phi_a + 1/\phi_b]} \quad (B5)$$

Using these equations with the dimensions indicated above for the monomer and dimer molecules we find that $R \equiv \phi_M/\phi_D \approx 0.69$.

References

- [1] J. Borejdo, S. Putnam and M.F. Morales, Proc. Natl. Acad. Sci. USA, 76 (1979) 6346–6350.
- [2] J. Borejdo, O. Assulin, T. Ando and S. Putnam, J. Mol. Biol., 158 (1982) 391–414.
- [3] T.P. Burghardt, T. Ando and J. Borejdo, Proc. Natl. Acad. Sci. USA, 80 (1983) 7515–7519.

- [4] T.P. Burghardt and K. Ajtai, *Biochemistry*, 33 (1994) 5376–5381.
- [5] K. Ajtai, D.J. Toft and T.P. Burghardt, *Biochemistry*, 33 (1994) 5382–5391.
- [6] K. Ajtai, P.J.K. Ilich, A. Ringler, S.S. Sedarous, D.J. Toft and T.P. Burghardt, *Biochemistry*, 31 (1992) 12431–12440.
- [7] R.W. Chambers, T. Kijiwara and D.R. Kearns, *J. Phys. Chem.*, 78 (1974) 380–387.
- [8] J.E. Selwyn and J.I. Steinfeld, *J. Phys. Chem.*, 76 (1972) 762–774.
- [9] I. López Arbeloa and P. Ruiz Ojeda, *Chem. Phys. Lett.*, 87 (1982) 556–560.
- [10] J.A. Schellman, *Chem. Rev.*, 75 (1975) 323–331.
- [11] C.R. Cantor and P.R. Schimmel, *Biophysical Chemistry, Part II*, Freeman, New York, 1980, pp. 409–590.
- [12] S. Bloński, *Chem. Phys. Lett.*, 184 (1991) 229–234.
- [13] R.L. Fulton and M. Gouterman, *J. Chem. Phys.*, 35 (1961) 1059–1071.
- [14] R.L. Fulton and M. Gouterman, *J. Chem. Phys.*, 41 (1964) 2280–2286.
- [15] J.B. Segur, in C.S. Miner (Ed.), *Glycerol, Physical Properties of Glycerol and its Solutions*, Reinhold, New York, 1953, p. 322.
- [16] Th. Förster, *Z. Naturforsch.*, 4a (1949) 321–327.
- [17] D.E. Koppel, P.J. Fleming and P. Strittmatter, *Biochemistry*, 18 (1979) 5450–5457.
- [18] Th. Förster, in D. Sinanoğlu (Ed.), *Modern Quantum Chemistry, Decocalized Excitation and Excitation Transfer*, Academic Press, New York, 1965, pp. 93–137.
- [19] M.E. Gál, G.R. Kelly and T. Kurucsev, *J. Chem. Soc. Faraday Trans. II*, (1973) 395–402.